Articles

Scanning Tunneling Spectroscopy of Individual PbSe Quantum Dots and Molecular Aggregates Stabilized in an Inert Nanocrystal Matrix

Karin Overgaag, Peter Liljeroth, Bruno Grandidier, and Daniël Vanmaekelbergh

ACS Nano, **2008**, 2 (3), 600-606 • DOI: 10.1021/nn7003876 • Publication Date (Web): 06 March 2008

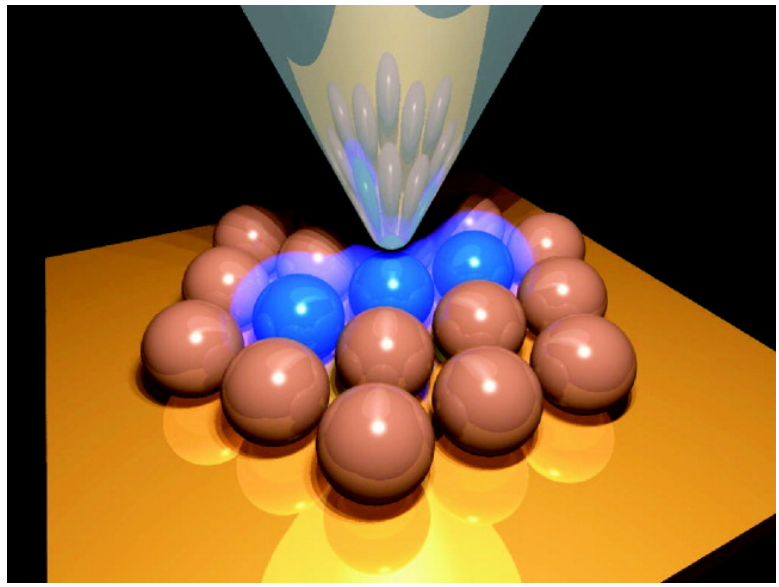

ARTICLE

Scanning Tunneling Spectroscopy of Individual PbSe Quantum Dots and Molecular Aggregates Stabilized in an Inert Nanocrystal Matrix

Karin Overgaag,[†,*] Peter Liljeroth,[†,‡] Bruno Grandidier,[§] and Daniël Vanmaekelbergh[†]

[†]Condensed Matter and Interfaces, Debye Institute, Utrecht University, P.O. Box 80 000, 3508 TA Utrecht, The Netherlands, [§]Institut d'Electronique, de Microélectronique et de Nanotechnology, Département ISEN, 41 boulevard Vauban, F-59046 Lille Cedex, France. [‡]Present address: IBM Zurich Research Laboratory, CH-8803 Rüschlikon, Switzerland.

ABSTRACT The electronic local density of states (LDOS) of single PbSe quantum dots (QDs) and QD molecules is explored using low-temperature scanning tunneling microscopy (STM) and spectroscopy (STS). Both individual PbSe QDs and molecular aggregates of PbSe QDs (dimers, trimers, *etc.*) are mechanically stabilized in a two-dimensional superlattice of wide band gap CdSe QDs acting as an inert matrix. The LDOS measured at individual QDs dispersed in the matrix is identical to that of single isolated QDs chemically linked to a substrate. We investigate the degree of quantum mechanical coupling between the PbSe QDs in molecular aggregates by comparing the LDOS measured at each site in the aggregates to that of an individual PbSe QD. We observe a variable broadening of the resonances indicating a spatially dependent degree of electron delocalization in the molecular aggregates.

KEYWORDS: scanning tunneling microscopy (STM) · scanning tunneling spectroscopy (STS) · colloidal quantum dots (QDs) · quantum mechanical coupling · QD molecules

Colloidal nanocrystalline quantum dots (QDs) play a key role in current nanoscience. These semiconductor nanocrystals, 1–10 nm in size, show strong quantum confinement resulting in size-tunable optical and electrical properties. There is a strong belief that such semiconductor nanocrystals will form the building blocks for QD solids with novel optical or electrical properties.[1–5] These properties will depend on the nature of the QD building blocks and the degree of electronic coupling between them. Optical and electrical spectroscopies have been used to characterize nanostructures; however, they can only measure sample-averaged properties. These techniques cannot answer an important question regarding nanostructured materials: the relation between the local atomic and electronic structure and the macroscopic (system-averaged) properties. This implies that the local interactions between the nanoscale building blocks should be measured. This aim can be reached through the use of local probes, in particular scanning tunneling microscopy (STM) and spectroscopy (STS), which can measure topography and electronic structure with very high spatial resolution. The combination of STM and STS has already proved very useful in probing the geometry and electronic structure of individual atoms and molecules and molecular aggregates at the atomic scale.[6–12] Furthermore, these techniques have been successfully used for the investigation of individual InAs, CdSe, and PbSe QDs,[13–17] as well as their two-dimensional arrays.[18,19] In order to study a single, isolated QD or small aggregates of QDs with STM, they have to be immobilized on a conducting substrate. This is typically achieved using functionalized organic molecules to chemically link nanocrystal QDs to the substrate. A good control of the surface chemistry is required to get stable substrate/QD/tip junctions. Moreover, some uncertainty remains concerning the extent to which covalent linking to a conducting substrate influences the electron and hole energy levels and electron and hole charging energies of the QDs.

Here, we propose an alternative method of stabilizing individual QDs and, in addition, realizing QD molecules: embedding the QDs of interest in a monolayer matrix of wider band gap nanocrystals of about the same size. We demonstrate this approach by studying PbSe QDs embedded in a monolayer of CdSe nanocrystals where the PbSe QDs can be identified by both topographic (STM) and spectroscopic (STS) measurements. The tunneling processes that occur during resonant tunneling spec-

*Address correspondence to k.overgaag@uu.nl.

Received for review November 27, 2007 and accepted February 12, 2008.

Published online March 6, 2008.
10.1021/nn7003876 CCC: $40.75

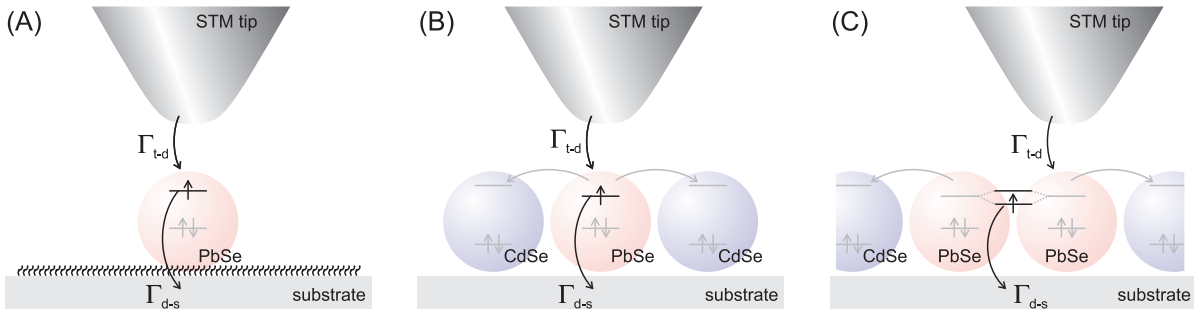

Figure 1. Schematic of the tunneling processes (denoted by arrows) that are possible with isolated PbSe QDs and QDs embedded in a matrix of CdSe QDs: (A) a single PbSe QD chemically linked to the substrate with hexanedithiol; (B) an isolated PbSe QD surrounded by CdSe QDs, in which the incoming electron can tunnel either directly or *via* neighboring CdSe QDs to the substrate; (C) the electronic levels in a PbSe QD dimer can be strongly coupled and the electron can delocalize over the two QDs. The subscripts t, d, and s stand for tip, dot, and substrate, and Γ corresponds to the tunneling rate.

troscopy for an isolated PbSe QD chemically linked to a substrate and a QD dispersed in a matrix are shown in Figure 1, parts A and B, respectively. In the first case, electrons injected from the tip into the QD can only tunnel out to the substrate. On the other hand, in an array, the injected electrons can tunnel out to the substrate or to the neighboring QDs in the matrix. This has an effect on the accessible regimes in tunneling spectroscopy, that is, shell-tunneling vs shell-filling conditions.[15,16]

As the PbSe QDs are dispersed in the CdSe monolayer, there is a distribution of monomers, dimers, and larger aggregates of PbSe QDs. This opens the possibility of studying electronic interactions between the PbSe QD building blocks in small "molecules". We observe significant quantum mechanical coupling between QDs and probe this coupling at the single QD level by performing STS on the different QD sites in the molecular aggregates. This gives information on the local variations of the quantum mechanical coupling resulting from disorder. In addition, the study of these systems complements the study of more extended 2D QD arrays.[18,19]

RESULTS AND DISCUSSION

We first discuss how PbSe QDs dispersed in a CdSe matrix can be detected by STM and STS. We then present spectroscopy of the energy levels of single PbSe QDs dispersed in an inert CdSe QD matrix, and finally discuss how electronic coupling in PbSe QD "molecules" can be quantified by STS.

Topographic Measurements of Mixed PbSe and CdSe QD Arrays. Figure 2A shows a topographic image of a self-assembled monolayer of CdSe QDs with an average diameter of 6.1 nm on a Au(111) substrate. The QD monolayers are very stable under STM imaging conditions (20–50 pA at 2.5 V). The monolayer shows local hexagonal packing but lacks true long-range order due to size, shape, and orientational disorder of the CdSe QDs. Mixing CdSe and PbSe QDs with a suitable concentration ratio results in PbSe nanocrystals dispersed in a matrix of CdSe. Figure 2B shows an STM image of 7.1 nm PbSe QDs dispersed in a CdSe matrix at a ratio of 1:30. The diameter of individual QDs chemically linked to a Au(111) substrate can be measured *in situ* by the STM height;[17] however, this is not possible for QDs in an array. We therefore use the average diameter of the PbSe QDs determined from transmission electron microscopy (TEM) measurements. We are able to distinguish between the two types of QDs: the PbSe QDs (indicated by black dots in Figure 2B) appear higher than CdSe. The height difference is not only due to the size difference between the different QDs because STM topography is also sensitive to electronic effects. However, due to the exponential dependence of the tunneling current on the distance, the measured height difference is mostly due to the size difference between the QDs. The inset of Figure 2B shows an aggregate of three PbSe

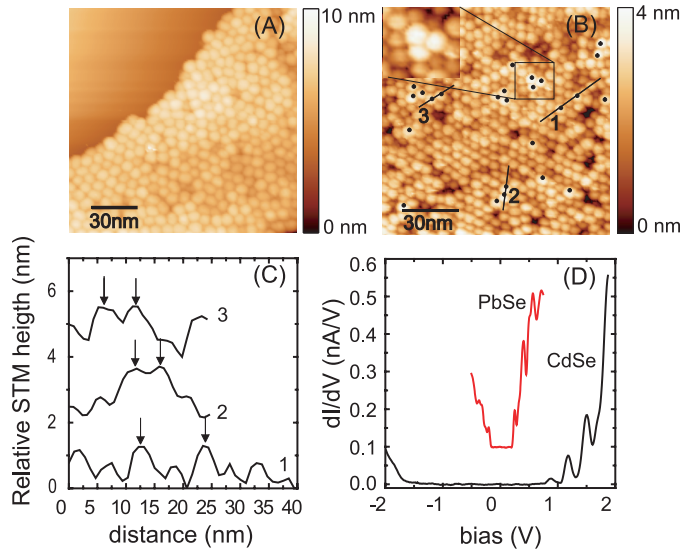

Figure 2. Topographic and spectroscopic identification of PbSe QDs in a CdSe QD matrix: (A) large scale STM image of a hexagonally packed monolayer of CdSe QDs with an average diameter of 6.1 nm (set-point current 10 pA and bias voltage 2.0 V); (B) STM image of 7.1 nm PbSe QDs (marked with black circles) dispersed in a matrix of 6.1 nm CdSe QDs (set-point current 30 pA at 2.5 V); (C) height profiles along the lines denoted in panel B; arrows indicate the PbSe nanocrystals; (D) examples of measured tunneling spectra (d*I*/d*V* vs *V*) at *T* = 5 K taken on an individual PbSe QD in a CdSe matrix (upper spectrum, off-set for clarity) and of a CdSe QD in the matrix (lower spectrum) with STS feedback settings 50 pA at 0.8 V (PbSe) and 150 pA at 2.0 V (CdSe).

TABLE 1. Experimental (f_{exp}) and Simulated (f_{rand}) Fractions of 9.8 nm Diameter PbSe QDs in Monomers, Dimers, *etc.* (N_{QD}) in a Matrix of 6.1 nm CdSe QDs for a PbSe/CdSe ratio of 1:10[a]

N_{QD}	f_{exp}	f_{rand}
1	0.086	0.536
2	0.064	0.266
3	0.046	0.122
4	0.033	0.054
5	0.058	0.023
6	0.038	0.008
7	0.036	0.005
8	0.020	0.001
9	0.017	0.000
10	0.026	0.000
>10	0.576	0.000

[a]The simulated values assume completely random assembly.

QDs in a matrix of CdSe QDs. Again, PbSe QDs appear clearly higher than the surrounding CdSe QDs. Figure 2C shows height profiles along the lines indicated in Figure 2B; there is a difference of about 1 nm between the larger PbSe (indicated with arrows) and smaller CdSe QDs, which is consistent with the difference in the core sizes measured by TEM. Comparison with the pure CdSe layer indicates that the size difference is sufficiently small not to perturb the local hexagonal ordering in the array.

The PbSe and CdSe QDs also have strikingly different LDOS, in particular in terms of the band gap. This allows us to easily identify the QDs by performing tunneling spectroscopy on them as illustrated in Figure 2D, where the difference in the electronic structure is apparent. For instance, the PbSe QDs have a much smaller zero-conductivity gap (related to the HOMO–LUMO band gap) than CdSe QDs. The interesting details of the electronic structure of individual PbSe QDs will be discussed in the following section.

Self-assembly of mixed QDs results in PbSe QDs dispersed in the CdSe QD matrix; there is a distribution of monomers, dimers, and larger aggregates. The STM can be used to identify the PbSe QDs either by topographic or by spectroscopic measurements. We have analyzed a series of STM images of 9.8 nm diameter PbSe QDs in a matrix of 6.1 nm CdSe QDs; the results are shown in Table 1 for a PbSe/CdSe ratio of 1:10. Comparison of the experimental and simulated (assuming completely random assembly) fractions shows that there are significant interactions between the PbSe QDs. Based on random assembly, we would expect a much larger fraction of monomers. In addition, we observe roughly half of the PbSe QDs to phase separate from the CdSe nanocrystals.

Spectroscopy of Single PbSe QDs in a CdSe Array. We have studied the electronic spectra of individual PbSe QDs embedded in a CdSe matrix. Figure 3A,B shows two typical spectra obtained on individual PbSe QDs with diameters of 7.1 and 9.8 nm embedded in a CdSe matrix. For comparison, Figure 3C presents a spectrum acquired over an isolated PbSe QD chemically anchored to the substrate. The spectra measured on these individual PbSe QDs show resonances from tunneling through valence (negative bias) and conduction levels (positive bias) separated by the zero-conductance gap. As expected, the zero-conductance gap and the level separations (*e.g.*, e_1 to e_2) decrease as the size of the QDs is increased from 7.1 to 9.8 nm. The spectra shown in Figure 3 were acquired at low set-point currents. However, the spectra remained unaffected on decreasing the tip/QD distance. It was possible to increase the current up to 2000 pA without any changes in the energy of the resonances. Based on this and earlier results,[14–16,18] we can conclude that the spectra shown in Figure 3 are shell-tunneling spectra; that is, the overall tunneling rate is limited by the tunneling rate between the tip and the QD. In this regime, electrons tunnel through the QD one-by-one, Coulomb interactions are absent, and the measured d*I*/d*V* spectrum directly reflects the single-particle LDOS of the QD. This is different from the spectroscopy on single CdSe nanocrystals chemically linked to a Au substrate where shell-tunneling spectra evolve into (partial) shell-filling when the current is increased.[14–16,20,21] The difference can be rationalized by two effects: due to the low effective masses of the carriers, the electronic orbitals of PbSe are more extended compared with CdSe, which results in larger tunneling coupling (tunneling rate Γ_{d-s}) be-

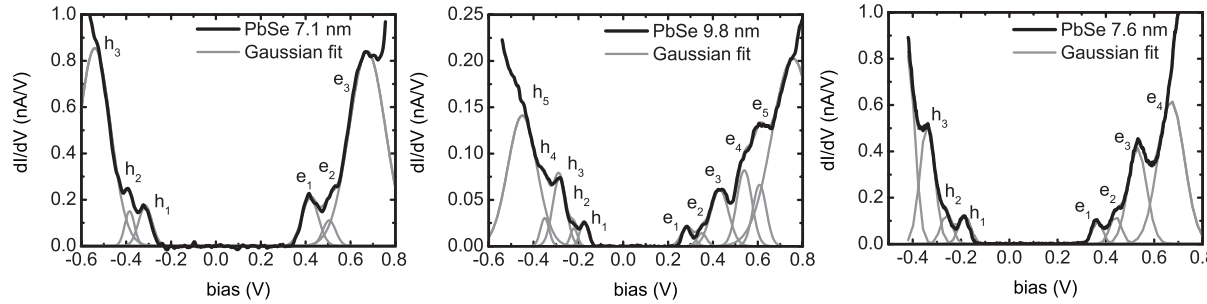

Figure 3. Spectroscopy on individual PbSe QDs with diameters of (A) 7.1 nm and (B) 9.8 nm embedded in a CdSe QD matrix. STS settings are 200 pA, 0.8 V, and 50 pA, 0.8 V, respectively. (C) Tunneling spectrum measured on a single PbSe nanocrystal (diameter 7.6 nm) chemically linked to Au(111) with hexanedithiol, set-point 200 pA and bias 0.8 V. The spectra are fitted with Gaussians and the resonances are denoted h_1 to h_5 for valence levels and e_1 to e_5 for the conduction levels. All spectra are measured at $T = 5$ K.

tween the QD and the substrate. In addition, the neighboring QDs can act as additional tunneling channels for electron escape. In the case of an isolated QD (Figure 1A), the system can be described as a QD in a double-barrier junction; the injected electron (rate $\Gamma_{in} = \Gamma_{t-d}$) can only leave the QD by tunneling from the dot into the gold substrate (rate $\Gamma_{out} = \Gamma_{d-s}$). The electron occupation is given by $\Gamma_{in}/(\Gamma_{in} + \Gamma_{out})$. It has been shown that this occupation factor can significantly differ from zero at high injection currents.[13,16] In the case of a QD in a matrix (Figure 1B), the rate of electron injection remains as $\Gamma_{in} = \Gamma_{t-d}$, while the rate of electron extraction $\Gamma_{out} = \Gamma_{d-s} + n\Gamma_{d-d}$ (n is the number of nearest neighbors). As a result, shell-filling is not observed even for high set-point currents; that is, $\Gamma_{in} \ll \Gamma_{out}$ for all injection currents.

The second remarkable difference in microscopy of an isolated QD chemically anchored to a substrate and a QD in an array is the stability of the latter junction. Isolated dots become unstable at high currents or voltages.[22] In contrast, the QDs in an array remain stable even when tunneling spectroscopy is performed under high set-point currents. The difference can be explained by the mechanisms of stabilization: in the case of an isolated dot, some of the chemical bonds between the QD or the substrate and the bifunctional linker molecules can be broken or weakened due to inelastic scattering of the tunneling electrons or the occupation of antibonding orbitals.[22] On the other hand, the QDs in an array are stabilized by the sum of the van der Waals interactions between the nanocrystal under the tip and its neighbors and the gold substrate; these interactions are not affected by the voltage or tunneling events.

The spectra in Figure 3 have been fitted with a sum of Gaussians, one for each resonance. The resonances are labeled h_1 to h_5 at negative bias (hole levels) and e_1 to e_5 at positive bias (electron levels). The resonances e_1 and h_1 stand for the lowest electron and hole level, respectively, with s-type envelope symmetry. The widths of the resonances (corrected for the effect of the potential distribution in the double-barrier junction[16,20,21,23]) increase considerably with decreasing QD size (For the first resonance fwhm (e_1) = 34 meV for 9.8 nm diameter and 55 meV for 7.1 nm). There are several factors that contribute to level broadening. Temperature and lifetime (controlled by the tunneling rate out of the QD) are obvious factors; however, these both are negligibly small (<1 meV) at $T = 5$ K and for the experimental junction geometry. Other factors include electron–phonon coupling and local heating effects. The former involves coupling of the tunneling electrons to either optical phonons of the nanocrystal core or vibrational modes of the capping molecules. The latter is proportional to the rate of inelastic tunneling events. In PbSe, there is an additional source of broadening for the tunneling resonances. The fundamental gap is at the L-point of the Brillouin zone and hence 4-fold degenerate.[24,25] However, the different valleys in the Brillouin zone are coupled ("intervalley coupling"), and this lifts the 4-fold degeneracy of the s-states for electrons and holes, and the levels split. This splitting depends on the size of the crystal and is larger for smaller nanocrystals. Tight-binding and pseudopotential calculations predict splittings on the order of a few tens of millielectronvolts depending on the size of the QDs.[24,25] In tunneling spectroscopy, the intrinsic line width (given by the other effects discussed above) is larger than this splitting, and hence, the different s-levels cannot be observed as separate resonances.

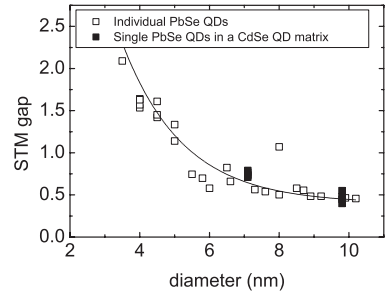

Figure 4. Comparison between the observed STM gap (e_1-h_1) as function of PbSe QD diameter for individual QDs chemically linked to a Au(111) substrate (□) and single PbSe QDs in a CdSe matrix (■). The diameter of the individual PbSe QDs is determined from the STM height. For the single PbSe QDs in the CdSe matrix, an average diameter of the PbSe QDs is determined from TEM images.

The resonances e_3 and h_3 stand for the p-type or d-type levels. The width of these resonances is considerably larger compared with e_1 and h_1. It is likely that the splitting of the p-levels is further increased due to the crystal dipole moment in PbSe.[26,27] It seems feasible that the weak but reproducible resonance e_2 corresponds to the lowest p-level. The spectra measured on single PbSe nanocrystals in a CdSe matrix are very similar to spectra measured on single PbSe nanocrystals chemically linked to a Au(111) substrate with hexanedithiol (Figure 3C).[17] In both cases, we get consistent results on the energy level positions as well as the widths of the resonances as is shown in Figure 4. This means that tunneling coupling between the PbSe QD and the surrounding CdSe QDs is sufficiently weak not to affect the tunneling spectra. Hence, immobilization of PbSe by a CdSe matrix proves to be a valuable method to study individual QDs and QD molecules of interest.

Spectroscopy on PbSe Aggregates in a CdSe Array. In addition to investigating isolated QDs, embedding PbSe QDs in the inert matrix allows us to study possible quantum mechanical coupling effects in small molecular aggregates of PbSe QDs. We will focus on 9.8 nm PbSe QDs: a dimer, a chain of four, and a larger aggregate of PbSe QDs as shown in the insets of Figures 5 and 6. First we investigate in more detail the LDOS measured on a dimer, two neighboring QDs of 9.8 nm embedded in a

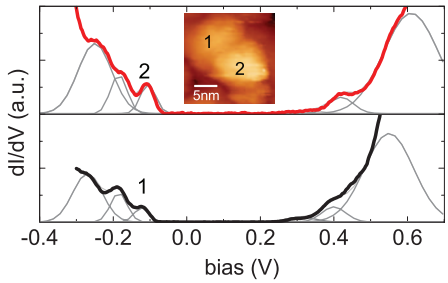

Figure 5. Spectroscopy on a 9.8 nm PbSe dimer embedded in a CdSe matrix. The thin lines represent Gaussian distributions fitted to the resonances. Spectra were measured at 5 K with set-point current 70 pA, bias 0.7 V (QD1) and 150 pA, 0.6 V (QD2).

CdSe matrix (Figure 5, inset). The spectra measured on this dimer are qualitatively similar to those on isolated QDs: zero-conductance gap and resonances at positive and negative bias resulting from tunneling through the valence and conductance levels. The resonance energy level positions did not change for set-point currents between 50 and 600 pA and bias 0.6 to 0.8 V. The full-width at half-maximum of the resonances corresponding to the hole levels (negative bias) is 35–40 meV, unchanged with respect to those of isolated PbSe QDs in a CdSe matrix. At positive bias however, the line width of the first electron resonance is 70 meV for QD1 and 75 meV for QD2, hence considerably broadened with respect to that of the single PbSe QD in a matrix (see Figure 3B). The broadening of the resonances is most likely caused by quantum mechanical interaction between PbSe QDs.[28] In a simple picture, this additional broadening of ca. 30 meV reflects the splitting of the conduction levels induced by coupling between the QDs. We use an elementary tight-binding scheme to compare the coupling in the QD dimer to the larger aggregates: the splitting of 30 meV corresponds to a value of $t_{d-d} = 15$ meV of the QD−QD coupling matrix element.[29]

We concentrate next on two examples of larger aggregates of PbSe QDs shown in Figure 6. The spectra in a linear aggregate of four PbSe QDs (Figure 6A) show that the line width of the first electron resonance of QDs 1, 2, and 3 are 53, 59, and 65 meV, respectively. This is again considerably broadened with respect to that of a single PbSe QD in an array of CdSe QDs (Figure 3B), which has a width of 35 meV. There is an extra peak in the d*I*/d*V* spectrum 3 in Figure 6A (at −0.17 V); the origin of this resonance is not presently clear. The feature is not visible for the other QDs in the same assembly, and hence, we have not included it in the fitting of the resonances. Coupling in this linear chain is smaller than that in the dimer shown in Figure 5; tight-binding considerations (equal coupling between all the QDs in the chain) gives $t_{d-d} \approx 10$ meV in this case.

In addition to small aggregates, we also investigated seven neighboring QDs in the middle of a larger aggregate containing only PbSe QDs, see Figure 6B. The QDs order in a hexagonal structure, as shown in the STM topography (inset). It is clear that the spectra differ from site to site. We again focus on the width of the first electron resonance; QD1 = 70 meV, QD2 = 94 meV, QD3 = 81 meV, QD4 = 88 meV QD5 = 87 meV, QD6 = 78 meV, and QD7 = 93 meV. From the above, it is clear that the electron resonances of PbSe QDs in a molecule show a variable broadening with respect to that of a single PbSe QD. In this larger structure, we can estimate an average coupling based on tight-binding, $t_{d-d} \approx 7$ meV. This assumes an infinite system, equal coupling between the QDs, and that the peak broadening is equal to the width of the band in tight binding. In only a few cases, the resonances of the valence hole levels are additionally broadened with respect to that of a single PbSe QD (see, for instance, Figure 6B QD5 and 6).

In Figure 7, we show the measured fwhm for the first conduction-level resonance for a number of monomers, dimers, *etc*. We can make the following conclusions based on the figure: (i) the line width increases when the number of PbSe QDs in the aggregate increases, (ii) the line width seems to saturate at about 90 meV, and (iii) there is considerable spread in the measured values from site-to-site in a given aggregate and from aggregate to aggregate. While points i and iii are rather obvious (more coupled QDs implies larger splitting of the levels), point ii gives valuable insight about the nature of coupling. It seems that the coupling strength is mainly determined by nearest-neighbor coupling and that disorder limits the size of the strongly coupled regions in larger assemblies. We can convert the measured fwhm to the QD−QD coupling matrix element t_{d-d}, and we find the following values: 14 meV for dimers, 14 meV for trimers, 12 meV for tetramers, and 6 meV for the larger assembly.

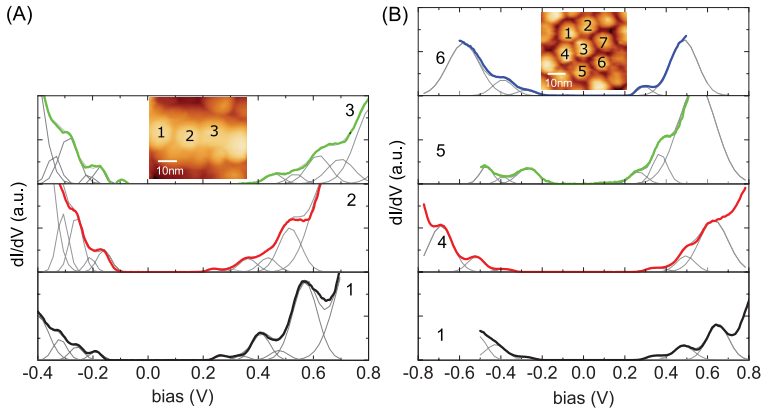

Figure 6. Spectroscopy on PbSe aggregates embedded in a CdSe matrix: (A) spectra measured on three QDs on a chain of four 9.8 nm diameter PbSe QDs—the thin solid lines represent Gaussian distributions fitted to the resonances (set-point current 100–350 pA and bias 0.7–1.8 V); (B) representative spectra on QDs that are part of a larger aggregate of 9.8 nm diameter PbSe QDs (set-point current 100–350 pA and bias 0.7–1.8 V). All spectra are measured at $T = 5$ K.

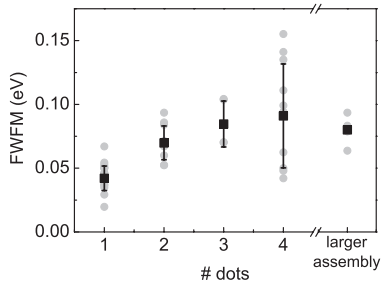

Figure 7. The measured fwhm (gray dots) of the tunneling resonance corresponding to the first conduction level as a function of the size of the PbSe QD aggregate and the average values with error bars (black squares, except for the larger assembly; we only have a data set for one aggregate and hence not sufficient statistics for an error estimate).

Despite electrons and holes having very similar effective masses in PbSe, we observe stronger coupling of the electron energy levels. This can be understood by considering the influence of the effective barrier height on the coupling strength: a difference of 2 eV for the electrons and holes is sufficient to accommodate the present results.[18] In the present system, the tunneling barrier is formed by the capping ligands. The barrier height for the electrons can be defined as the energy difference between the LUMO of the capping molecules and the first conduction level of the QDs, while for the holes, it is the energy difference between the HOMO of the capping ligands and the first valence level of the QDs. Exact values for these barrier heights are not known. However, lead chalcogenide materials are known to have low ionization potentials, which makes it more likely that the barrier height for electrons is lower than that for the holes.[30] This band-selective coupling is consistent with earlier results on extended arrays of PbSe and has also been observed for arrays of InAs QDs.[18,19] The variable broadening of the resonances that we observe from site to site indicates that the degree of quantum mechanical coupling is strongly site-dependent. It is likely that in extended arrays, strong coupling only prevails over areas of a few QDs. It must be realized that colloidal nanocrystals are faceted and are hence not perfectly spherical. This leads to several types of disorder; for instance, there might be variations in the orientation of the nanocrystals with respect to each other or small variations in the distance between the facets of the neighboring nanocrystals resulting in a variable degree of electronic coupling.

CONCLUSIONS

In conclusion, we have shown that we can prepare PbSe QD monomers, dimers, and larger aggregates dispersed in a matrix of CdSe QDs. Both CdSe and PbSe nanocrystals can be identified by scanning tunneling microscopy and spectroscopy. The CdSe QD array can be considered as an inert matrix stabilizing the dispersed PbSe QDs. The spectra of single PbSe QDs in the CdSe matrix are nearly identical to those of isolated PbSe QDs chemically anchored to the substrate. Small "molecules" of PbSe QDs dispersed in the CdSe matrix can also be investigated. We observe a variable degree of electron delocalization in the small aggregates with typical coupling strengths of 10−20 meV. The results in this paper show that QD arrays with two different types of building blocks can be quantitatively studied. It is possible to measure the local "atomic" configuration together with the LDOS. This is a promising prospect for further study of ordered binary QD solids, systems that are the focus of intense current interest.[31,32]

METHODS

The CdSe QDs serve as stabilizing matrix to investigate the electronic structure of single and aggregates of two or more PbSe QDs. The CdSe QDs are passivated by organic ligands (TOPO and HDA) and have a core diameter of 6.1 nm.[33] We used two different sizes of PbSe quantum dots (diameters 7.1 and 9.8 nm) capped with oleic acid.[2,27] The average diameter, shape, and size distribution (5–10%) of the QDs were determined by transmission electron microscopy (TEM) and optical spectroscopy.

Two-dimensional arrays were prepared by self-assembly. CdSe and PbSe nanocrystals dispersed in chloroform were drop-casted on flame-annealed Au(111). Control over the concentration ratio CdSe/PbSe led to monolayers of CdSe with dispersed individual PbSe QDs and also aggregates of two or more PbSe QDs.

Immediately after sample preparation (carried out under oxygen- and water-free conditions), the sample was inserted into the ultrahigh vacuum (UHV) system. Prior to the STM experiments, the samples were annealed in UHV up to 110 °C. Low-temperature STM (LT-STM Omicron Technology) operated at $T = 5$ K in UHV (base pressure $<10^{-10}$ mbar) was used to investigate the topography and electronic structure of these self-assembled structures. We used electrochemically etched tungsten tips, and the topography images were acquired in constant current mode, with typical imaging parameters being set-point current of 10–50 pA at a bias voltage (applied to the sample) of 2.5 V. The electronic density of states was obtained by positioning the STM tip above the center of the QD of interest and disconnecting the feedback loop. The tunnel current I was measured as a function of the bias V between the tip and the substrate. The conductance dI/dV was measured simultaneously using a lock-in amplifier (rms modulation 10 mV at 500 Hz) or by numerically differentiating the experimental $I-V$ curves. Typically, a large number of spectra (~ 100) were acquired above one QD. In general, the measured spectra were reproducible, although discrete shifts of the spectra along the bias axis were observed in some cases. Sets of reproducible $I-V$ and dI/dV spectra were averaged to increase the signal-to-noise ratio, which did not affect the width of the resonances in the spectra. We carried out a detailed set of experiments on 11 monomers, 4 dimers, 2 trimers, 2 tetramers, and 1 larger assembly where seven QDs were investigated.

The fitting procedure for the dI/dV spectra of the PbSe QD aggregates starts with the number and position of Gaussian peaks used to fit the spectra of isolated PbSe QDs. Because there is some uncertainty in fitting the higher order resonances, we only use the first resonance in determining the coupling strength.

Acknowledgment. P.L. wishes to acknowledge financial support from NWO/Chemical Sciences (Vidi-grant 700.56.423). We are thankful to Rolf Koole, Arjan Houtepen, and Celso de Mello Donegá for the nanocrystal samples used in this study.

REFERENCES AND NOTES

1. Redl, F. X.; Cho, K. S.; Murray, C. B.; O'Brien, S. Three-Dimensional Binary Superlattices of Magnetic Nanocrystals and Semiconductor Quantum Dots. *Nature* **2003**, *423*, 968–971.
2. Murray, C. B.; Sun, S.; Gaschler, W.; Doyle, H.; Betley, T. A.; Kagan, C. R. Colloidal Synthesis of Nanocrystals and Nanocrystal Superlattices. *IBM J. Res. Dev.* **2001**, *45*, 47–56.
3. Vanmaekelbergh, D.; Liljeroth, P. Electron-Conducting Quantum Dot Solids: Novel Materials Based on Colloidal Semiconductor Nanocrystals. *Chem. Soc. Rev.* **2005**, *34*, 299–312.
4. Yin, Y.; Alivisatos, A. P. Colloidal Nanocrystal Synthesis and the Organic - Inorganic Interface. *Nature* **2005**, *437*, 664–670.
5. Murray, C. B.; Kagan, C. R.; Bawend, M. G. Synthesis and Characterisation of Monodisperse Nanocrystals and Close-Packed Nanocrystal Assemblies. *Annu. Rev. Mater. Sci.* **2000**, *30*, 545–610.
6. Olsson, F. E.; Persson, M.; Borisov, A. G.; Garyacq, J. P.; Laqoute, J.; Fölsch, S. Localization of the Cu(111) Surface State by Single Cu Adatoms. *Phys. Rev. Lett.* **2004**, *93*, 206803/1–4.
7. Repp, J.; Meyer, G.; Paavilainen, S.; Olsson, F. E.; Persson, M. Scanning Tunneling Spectroscopy of Cl Vacancies in NaCl Films: Strong Electron-Phonon Coupling in Double-Barrier Tunneling Junctions. *Phys. Rev. Lett.* **2005**, *95*, 225503/1–4.
8. Qiu, X. H.; Nazin, G. V.; Ho, W. Vibronic States in Single Molecule Electron Transport. *Phys. Rev. Lett.* **2004**, *92*, 206102/1–4.
9. Silien, C.; Pradhan, N. A.; Ho, W.; Thiry, P. A. Influence of Adsorbate-Substrate Interaction on the Local Electronic Structure of C60 Studied by Low-Temperature STM. *Phys. Rev. B* **2004**, *69*, 115434/1–5.
10. Lu, X.; Grobis, M.; Khoo, K. H.; Louie, S. G.; Crommie, M. F. Charge Transfer and Screening in Individual C60 Molecules on Metal Substrates: A Scanning Tunneling Spectroscopy and Theoretical Study. *Phys. Rev. B* **2004**, *70*, 115418/1–8.
11. Liljeroth, P.; Repp, J.; Meyer, G. Current-Induced Hydrogen Tautomerization and Conductance Switching of Naphthalocyanine Molecules. *Science* **2007**, *317*, 1203–1206.
12. Venema, L. C.; Wildoer, J. W. G.; Tans, S. J.; Janssen, J. W.; Temminck Tuinstra, H. L. W.; Kouwenhoven, L. P.; Dekker, C. Imaging Electron Wave Functions of Quantized Energy Levels in Carbon Nanotubes. *Science* **1999**, *283*, 52–55.
13. Banin, U.; Cao, Y.; Katz, D.; Millo, O. Identification of a Atomic-Like Electronic States in Indium Arsenide Nanocrystal Quantum Dots. *Nature* **1999**, *400*, 542–544.
14. Banin, U.; Millo, O. Tunneling and Optical Spectroscopy of Semiconductor Nanocrystals. *Annu. Rev. Phys. Chem.* **2003**, *54*, 465–492.
15. Bakkers, E. P. A. M.; Hens, Z.; Zunger, A.; Franceschetti, A.; Kouwenhoven, L. P.; Gurevich, L.; Vanmaekelbergh, D. Shell-Tunneling Spectroscopy of the Single-Particle Energy Levels of Insulating Quantum Dots. *Nano Lett.* **2001**, *1*, 551–556.
16. Jdira, L.; Liljeroth, P.; Stoffels, E.; Vanmaekelbergh, D.; Speller, S. Size-Dependent Single-Particle Energy Levels and Interparticle Coulomb Interactions in CdSe Quantum Dots Measured by Scanning Tunneling Spectroscopy. *Phys. Rev. B* **2006**, *73*, 115305/1–6.
17. Liljeroth, P.; Zeijlmans van Emmichoven, P. A.; Hickey, S. G.; Weller, H.; Grandidier, B.; Allan, G.; Vanmaekelbergh, D. Density of States Measured by Scanning-Tunneling Spectroscopy Sheds New Light on the Optical Transitions in PbSe Nanocrystals. *Phys. Rev. Lett.* **2005**, *95*, 086801/1–4.
18. Liljeroth, P.; Overgaag, K.; Urbieta, A.; Grandidier, B.; Hickey, S. G.; Vanmaekelbergh, D. Variable Orbital Coupling in a Two-Dimensional Quantum-Dot Solid Probed on a Local Scale. *Phys. Rev. Lett.* **2006**, *97*, 096803/1–4.
19. Steiner, D.; Azulai, D.; Aharoni, A.; Banin, U.; Millo, O. Level Structure of InAs Quantum Dots in Two-Dimensional Assemblies. *Nano Lett.* **2006**, *6*, 2201–2205.
20. Liljeroth, P.; Jdira, L.; Overgaag, K.; Grandidier, B.; Speller, S.; Vanmaekelbergh, D. Can Scanning Tunnelling Spectroscopy Measure the Density of States of Semiconductor Quantum Dots. *Phys. Chem. Chem. Phys.* **2006**, *8*, 3845–3850.
21. Niquet, Y. M.; Delerue, C.; Allan, G.; Lannoo, M. Interpretation and Theory of Tunneling Experiments on Single Nanostructures. *Phys. Rev. B* **2002**, *65*, 165334/1–14.
22. Hens, Z.; Talapin, D. V.; Weller, H.; Vanmaekelbergh, D. Breaking and Restoring a Molecularly Bridged Metal/Quantum Dot Junction. *Appl. Phys. Lett.* **2002**, *81*, 4245–4247.
23. For PbSe QDs in a matrix of CdSe, we estimate that $(V_{dot} - V_{tip})/V_{bias} = 0.85$ based on the solution of the Poisson equation for the tip/QD/substrate configuration. This means that the bias scale can be converted to an energy scale by multiplying by 0.85.
24. Allan, G.; Delerue, C. Confinement Effects in PbSe Quantum Wells and Nanocrystals. *Phys. Rev. B* **2004**, *70*, 245321/1–9.
25. An, J. M.; Franceschetti, A.; Dudiy, S.; Zunger, A. The Peculiar Electronic Structure of PbSe Quantum Dots. *Nano Lett.* **2006**, *6*, 2728–2735.
26. Shevchenko, E. V.; Talapin, D. V.; Murray, C. B.; O'Brien, S. Structural Characterization of Self-Assembled Multifunctional Binary Nanoparticle Superlattices. *J. Am. Chem. Soc.* **2006**, *128*, 3620–3637.
27. Houtepen, A. J.; Koole, R.; Vanmaekelbergh, D.; Meeldijk, J.; Hickey, S. G. The Hidden Role of Acetate in the PbSe Nanocrystal Synthesis. *J. Am. Chem. Soc.* **2006**, *128*, 6792–6793.
28. The factors contributing to the intrinsic line width of the transitions in the tunneling spectra, namely, strong electron−phonon coupling or local heating effects, should diminish with increasing size of the system. Hence, they are not responsible for the broadening that we observe with the coupled PbSe QDs.
29. Aschcroft, N. W.; Mermin, N. D., *Solid State Physics*; Saunders College Publishing: Fort Worth, TX, 1976.
30. McDonald, S. A.; Konstantatos, G.; Zhang, S.; Cyr, P. W.; Klem, E. J. D.; Levina, L.; Sargent, E. H. Solution-Processed PbS Quantum Dot Infrared Photodetectors and Photovoltaics. *Nat. Mater.* **2005**, *4*, 138–142.
31. Shevchenko, E. V.; Talapin, D. V.; Kotov, N. A.; O'Brien, S.; Murray, C. B. Structural Diversity in Binary Nanoparticle Superlattices. *Nature* **2006**, *439*, 55–59.
32. Urban, J. J.; Talapin, D. V.; Shevchenko, E. V.; Kagan, C. R.; Murray, C. B. Synergism in Binary Nanocrystal Superlattices Leads to Enhanced p-Type Conductivity in Self-Assembled PbTe/Ag2Te Thin Films. *Nat. Mater.* **2007**, *6*, 115–121.
33. de Mello Donegá, C.; Hickey, S. G.; Wuister, S. F.; Vanmaekelbergh, D.; Meijerink, A. Single-Step Synthesis to Control the Photoluminescence Quantum Yield and Size Dispersion of CdSe Nanocrystals. *J. Phys. Chem. B* **2003**, *107*, 489–496.